scientific reports

Check for updates

OPEN

Andrographolide promotes hippocampal neurogenesis and spatial memory in the APPswe/PS1ΔE9 mouse model of Alzheimer's disease

Sebastian B. Arredondo[1], Daniel T. Reyes[1], Andrea Herrera-Soto[1], Muriel D. Mardones[1], Nibaldo C. Inestrosa[2,3]✉ & Lorena Varela-Nallar[1]✉

In Alzheimer´s disease (AD) there is a reduction in hippocampal neurogenesis that has been associated to cognitive deficits. Previously we showed that Andrographolide (ANDRO), the main bioactive component of *Andrographis paniculate*, induces proliferation in the hippocampus of the APPswe/PSEN1ΔE9 (APP/PS1) mouse model of AD as assessed by staining with the mitotic marker Ki67. Here, we further characterized the effect of ANDRO on hippocampal neurogenesis in APP/PS1 mice and evaluated the contribution of this process to the cognitive effect of ANDRO. Treatment of 8-month-old APP/PS1 mice with ANDRO for 4 weeks increased proliferation in the dentate gyrus as evaluated by BrdU incorporation. Although ANDRO had no effect on neuronal differentiation of newborn cells, it strongly increased neural progenitors, neuroblasts and newborn immature neurons, cell populations that were decreased in APP/PS1 mice compared to age-matched wild-type mice. ANDRO had no effect on migration or in total dendritic length, arborization and orientation of immature neurons, suggesting no effects on early morphological development of newborn neurons. Finally, ANDRO treatment improved the performance of APP/PS1 mice in the object location memory task. This effect was not completely prevented by co-treatment with the anti-mitotic drug TMZ, suggesting that other effects of ANDRO in addition to the increase in neurogenesis might underlie the observed cognitive improvement. Altogether, our data indicate that in APP/PS1 mice ANDRO stimulates neurogenesis in the hippocampus by inducing proliferation of neural precursor cells and improves spatial memory performance.

Alzheimer's disease (AD) is the most common cause of dementia with an estimated prevalence of 30 million people worldwide[1]. AD is a neurodegenerative disorder characterized by a progressive memory loss, impaired cognitive functions, massive neuronal loss and synaptic dysfunction[2]. Neuropathological hallmarks of AD include extracellular amyloid plaques formed by deposition of amyloid β peptide (Aβ) generated from amyloid precursor protein (APP) processing, and intracellular neurofibrillary tangles mainly composed by hyperphosphorylated tau protein[2,3]. In addition to neuronal loss, a decline in hippocampal neurogenesis was observed in AD patients[4–6], which has also been evidenced in different animal models of the disease[7–10]. Interestingly, in AD mouse models impaired neurogenesis precedes Aβ plaque and neurofibrillary tangles formation[8,9,11,12]. This indicates that the impairment in neurogenesis is an early event in the disease progression, which has also been suggested in AD patients, where the decline in neurogenesis was observed even in individuals at early stages of the disease[4].

In the adult hippocampus, new neurons are generated from neural stem cells (NSCs) located at the subgranular zone (SGZ) in the dentate gyrus. These cells proliferate giving rise to neural progenitor cells (NPCs) that differentiate into neuroblasts that develop and mature into granule neurons that became integrated into

[1]Institute of Biomedical Sciences, Faculty of Medicine and Faculty of Life Sciences, Universidad Andres Bello, Echaurren 183, 8370071 Santiago, Chile. [2]Centro de Envejecimiento y Regeneración (CARE UC), Facultad de Ciencias Biológicas, Pontificia Universidad Católica de Chile, Av. Bernardo O´Higgins 340, P.O. Box 340-D, Santiago, Chile. [3]Centro de Excelencia en Biomedicina de Magallanes (CEBIMA), Universidad de Magallanes, Punta Arenas, Chile. ✉email: ninestrosa@bio.puc.cl; lorena.varela@unab.cl

Figure 1. ANDRO increases cell proliferation in the dentate gyrus of APPswe/PSEN1ΔE9 mice. (**A**) Schematic representation of experimental procedure; 8-month-old APPswe/PSEN1ΔE9 mice were injected i.p. with 2 mg kg^{-1} ANDRO or vehicle solution 3 times a week for 4 weeks. Animals received a daily i.p. injection of 100 mg kg^{-1} BrdU the last 3 days of treatment and were sacrificed 24 h after the last BrdU injection (a) or received a daily i.p. injection of 100 mg kg^{-1} BrdU for 3 consecutive days and were sacrificed 14 days after the first BrdU injection (b). (**B**) Representative confocal images of the immunofluorescence of Ki67 in the dentate gyrus of control wild-type (WT), APPswe/PSEN1ΔE9 (APP/PS1) mice, and APP/PS1 mice treated with ANDRO. Images correspond to maximal projection of 10 µm z-stack. Scale Bar: 50 µm. Right panels show higher magnifications of single z-stack of dotted squares shown in left panels. Arrows indicate Ki67-positive (Ki67+) cells. The graph shows the quantification of the total number of Ki67+ cells in the subgranular zone (SGZ). Data are presented as mean ± SEM; WT = 9 mice; APP/PS1 = 9 mice; APP/PS1 + ANDRO = 9 mice. *p = 0.0445; ***p = 0.0005, one-way ANOVA followed by Bonferroni post-hoc test. (**C**) Representative confocal images of the immunofluorescence of BrdU in the dentate gyrus of APPswe/PSEN1ΔE9 mice injected with vehicle solution (APP/PS1) and APP/PS1 mice treated with ANDRO. Images correspond to maximal projection of 8 µm z-stack. Scale Bar: 50 µm. Right panels show higher magnifications of single z-stack of dotted squares shown in left panels. Arrows indicate BrdU-positive (BrdU+) cells. The graph shows the quantification of the total number of BrdU+ cells in the SGZ. Data are presented as mean ± SEM; N = 3 mice. * p = 0.0177, unpaired Student's t-test.

the hippocampal circuitry[13–15]. Adult-born neurons contribute to hippocampal plasticity[16–19] and hippocampal-dependent tasks such as pattern separation, cognitive flexibility, and spatial learning and memory[20–22]. In humans, it was suggested a possible association between the extent of neurogenesis and cognitive status[5]. Therefore, the stimulation of neurogenesis has emerged as a possible therapeutic strategy in conditions affecting cognition.

Previously, we determined that Andrographolide (ANDRO), the main bioactive component of the medicinal plant *Andrographis paniculata*[23], induced hippocampal neurogenesis in adult mouse brain[24]. ANDRO is a labdane diterpenoid lactone that has multiple therapeutic uses. It has shown protective effects in animal models of cerebral ischemia[25], traumatic brain injury[26,27], and neurodegenerative diseases[28–32]. ANDRO treatment reduced cognitive impairment in APPswe/PS1ΔE9 and J20 transgenic mouse models of AD[30–32], as well as in *Octodon degus* used as a natural model of AD[33]. In addition, we determined that ANDRO induced cell proliferation in the hippocampus of APPswe/PS1ΔE9 mice[24]. Here we further characterized the effect of ANDRO treatment on hippocampal neurogenesis in APPswe/PS1ΔE9 mice and evaluated the potential contribution of neurogenesis in the effect of ANDRO on spatial memory improvement.

Results

ANDRO increases cell proliferation in the dentate gyrus of APPswe/PSEN1ΔE9 mice. Previously we determined that treatment with ANDRO increased the density of cells positive for the intrinsic proliferation marker Ki67 and for the immature neuronal marker doublecortin (DCX) in the dentate gyrus of APPswe/PSEN1ΔE9 mice[24]. Here, to further characterize the effect of ANDRO on neurogenesis we carried out two experimental designs (Fig. 1A): (a) To assess proliferation by nuclear incorporation of the nucleotide analog BrdU, 8-month-old APPswe/PSEN1ΔE9 mice were injected i.p. with 2 mg kg^{-1} ANDRO or vehicle solution 3 times a week for 4 weeks, the last 3 days of treatment animals received a daily i.p. injection of 100 mg kg^{-1} BrdU and were sacrificed 24 h after the last BrdU injection (Fig. 1A, a); (b) To evaluate neuronal differentiation of newborn cells, migration and development of newborn neurons, 8-month-old APPswe/PSEN1ΔE9 mice were injected i.p. with 2 mg kg^{-1} ANDRO or vehicle 3 times a week for 4 weeks, after 2 weeks of treatment the animals received a daily i.p. injection of 100 mg kg^{-1} BrdU for 3 consecutive days and were sacrificed 14 days after the first BrdU injection (Fig. 1A, b). In this experiment, age matched non-transgenic wild-type littermates receiving vehicle solution and BrdU were also included. In APPswe/PSEN1ΔE9 mice first pathological hallmarks of AD are detected at 4-month-old[34], and impairments in neurogenesis are evident as early as 2 months of age[11].

At the end of both experiments Ki67 staining was evaluated in the SGZ (Fig. 1B). A significant decrease in cells positive for Ki67 was observed in the dentate gyrus of APPswe/PSEN1ΔE9 mice compared to non-transgenic littermates (Fig. 1B), and as we previously reported[24], an increase in Ki67-positive cells was observed in APPswe/PSEN1ΔE9 mice treated with ANDRO (Fig. 1B). As expected, an increase in Ki67-positive cells was also observed in wild-type mice treated with ANDRO (control = 793 ± 89; ANDRO = 1102 ± 99, p = 0,048). Proliferation was also evaluated by incorporation of BrdU (Fig. 1A, a). A significant increase in the total number of BrdU-positive (BrdU+) cells was observed in the SGZ of APPswe/PSEN1ΔE9 mice treated with ANDRO compared with control APPswe/PSEN1ΔE9 mice injected with vehicle solution (Fig. 1C). This result strongly supports that ANDRO induces cell proliferation in the SGZ of APPswe/PSEN1ΔE9 mice.

ANDRO increases neural precursor cells and immature neurons in the dentate gyrus of APPswe/PSEN1ΔE9 mice. To evaluate the effect of ANDRO on neurogenesis we first evaluated cells positive for DCX (Fig. 2A), a microtubule-associated protein that is transiently expressed during maturation of newborn neurons[35]. Reduced number of DCX-positive (DCX+) cells was observed in the dentate gyrus of APPswe/PSEN1ΔE9 mice compared to age-matched wild-type mice, and a significant increase was observed in APPswe/PSEN1ΔE9 treated with ANDRO (Fig. 2B).

In addition, we evaluated the neural stem/progenitor cells and neuroblasts population (Fig. 2C). These cells were identified by immunostaining with GFAP, Sox2 and DCX, and by cell morphology[36,37]. NSCs, also known as type 1 cells, are positive for GFAP and Sox2 labeling and extend a radial process into the granule cell layer (GCL)

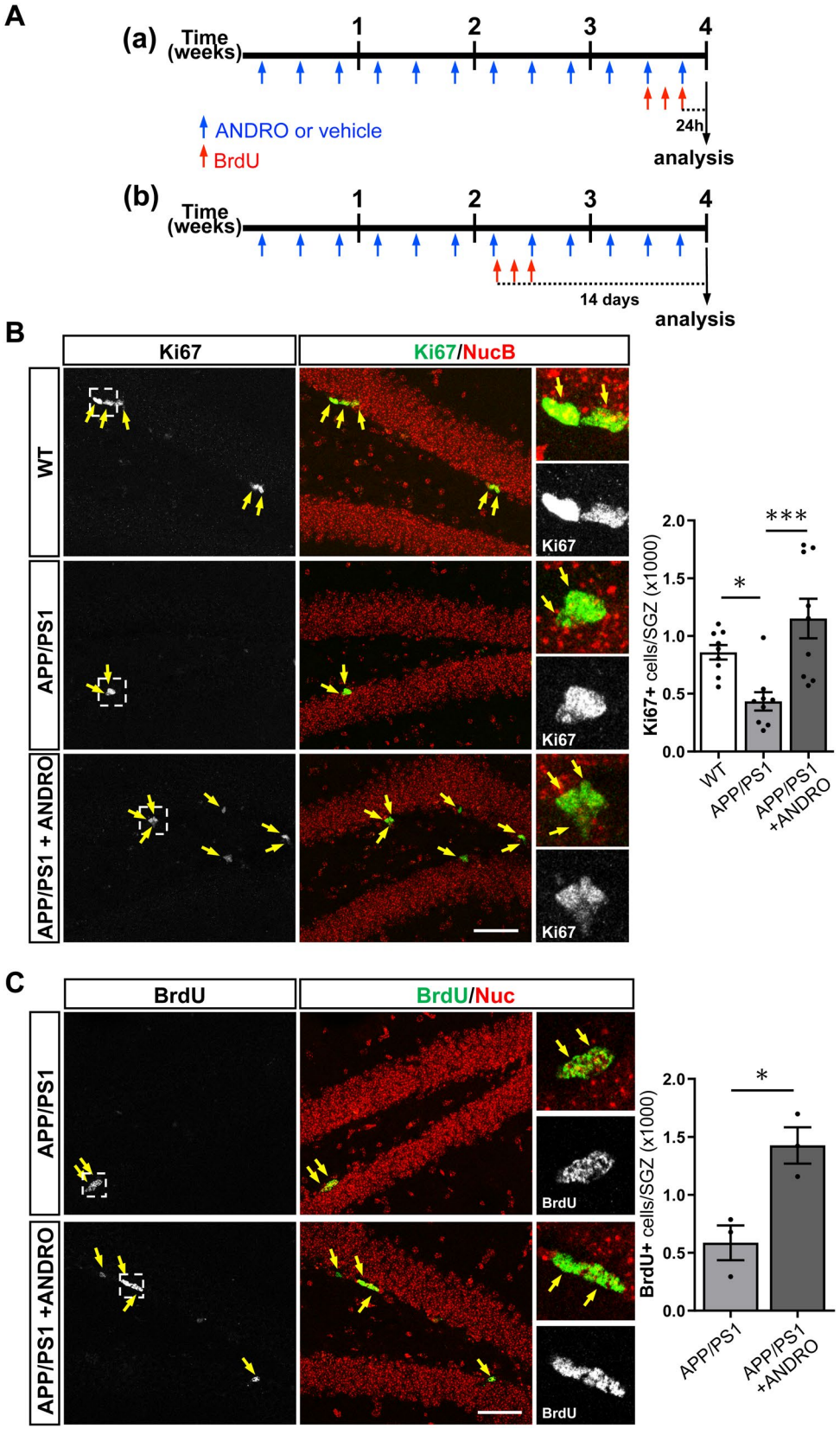
A
(a)
Time (weeks)
1
2
3
4
ANDRO or vehicle
BrdU
24h
analysis
(b)
Time (weeks)
1
2
3
4
14 days
analysis
B
Ki67
Ki67/NucB
WT
APP/PS1
APP/PS1 + ANDRO
Ki67
Ki67+ cells/SGZ (x1000)
2.0
1.5
1.0
0.5
0.0
*
***
WT
APP/PS1
APP/PS1 +ANDRO
C
BrdU
BrdU/Nuc
APP/PS1
APP/PS1 +ANDRO
BrdU
BrdU+ cells/SGZ (x1000)
2.0
1.5
1.0
0.5
0.0
*
APP/PS1
APP/PS1 +ANDRO

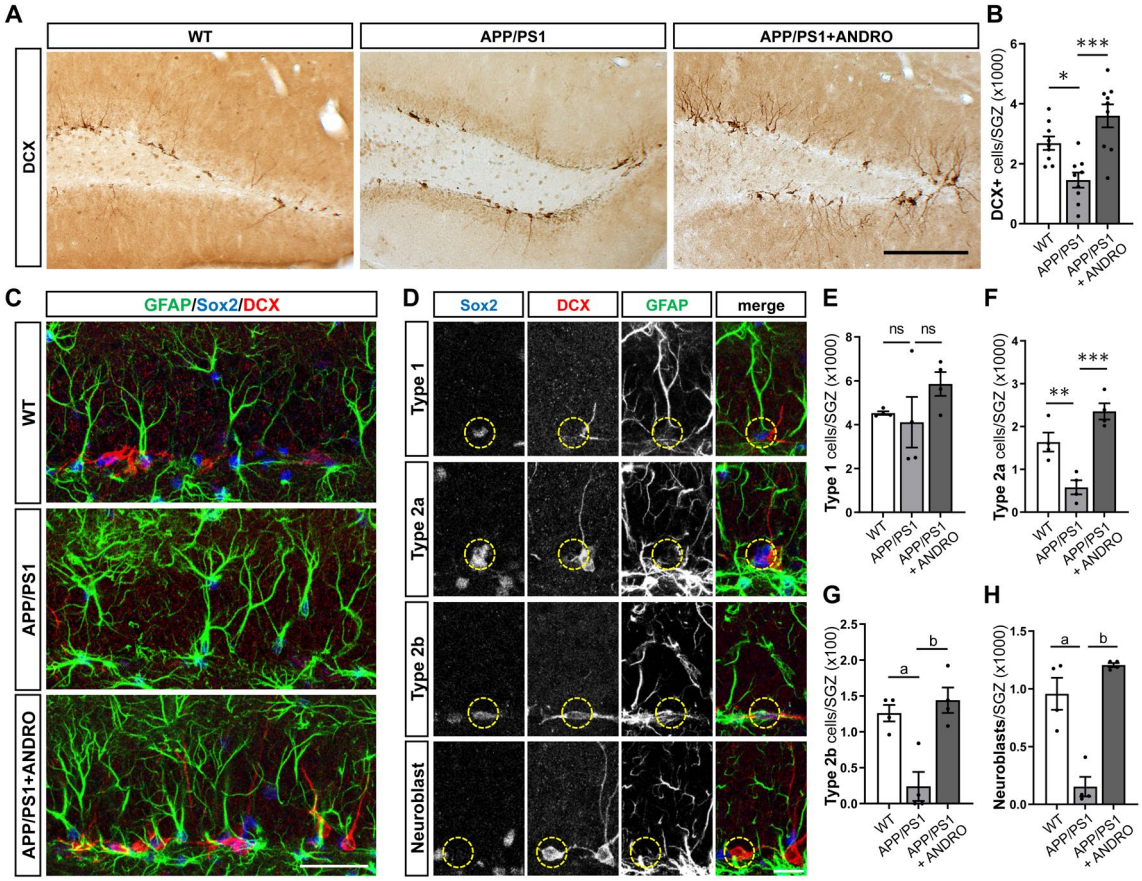

Figure 2. ANDRO increases neural precursor cells and immature neurons in the dentate gyrus of APPswe/PSEN1ΔE9 mice. (**A**) Representative immunostaining of immature neuronal marker DCX in the dentate gyrus of control wild-type (WT), APPswe/PSEN1ΔE9 (APP/PS1) mice, and APP/PS1 mice treated with ANDRO. Scale Bar: 200 µm. (**B**) Quantification of the total number of DCX+ cells in the granular cell layer (GCL). Data are presented as mean ± SEM; WT = 9 mice; APP/PS1 = 9 mice; APP/PS1 + ANDRO = 9 mice. *p = 0.0204, ***p < 0.0001, one-way ANOVA followed by Bonferroni post-hoc test. (**C**) Immunostaining of GFAP, Sox2 and DCX in WT, APP/PS1 mice, and APP/PS1 mice treated with ANDRO. Scale Bar: 40 µm. (**D**) Representative immunostaining of type 1, type 2a, type 2b cells and neuroblasts in the dentate gyrus identified by immunostaining with GFAP, Sox2 and DCX, and by cell morphology. Scale Bar: 20 µm. (**E–H**) Quantification of the total number of type 1 (**E**), type 2a (**F**), type 2b cells (**G**) and neuroblasts (**H**) in the SGZ of WT, APP/PS1, and APP/PS1 mice treated with ANDRO. Data are presented as mean ± SEM; WT = 4 animals; APP/PS1 = 4 animals; APP/PS1 + ANDRO = 4 animals. ns, non-significantly different. In (**F**), **p = 0.0098; ***p = 0.003. In (**G**), [a]p = 0.0062; [b]p = 0.0021. In (**H**), [a]p = 0.0006; [b]p < 0.0001; one-way ANOVA followed by Bonferroni post-hoc test.

(Fig. 2D). These cells divide to generate type 2 neural progenitors that are rounded cells located in the SGZ that do not express GFAP and that are classified as type 2a or type 2b cells based on their neuronal commitment[38]. Type 2a cells are positive for Sox2 but not for DCX labeling, while type 2b cells are positive for both, Sox2 and DCX (Fig. 2D). Neuroblasts are positive for DCX but negative for GFAP and Sox2 labeling (Fig. 2D), are located in the SGZ and may exhibit small horizontal processes[35]. No significant changes were observed in the number of type 1 cells between wild-type, APPswe/PSEN1ΔE9 mice and APPswe/PSEN1ΔE9 mice treated with ANDRO (Fig. 2E). A significant decrease was observed in type 2a, type 2b and neuroblasts in APPswe/PSEN1ΔE9 mice compared to wild-type mice (Fig. 2F–H), and the number of these cells was significantly increased by ANDRO treatment (Fig. 2F–H).

Altogether, these results indicate that although there are no differences in the NSC population, there is a reduced number of neural progenitors and immature neurons in the dentate gyrus of APPswe/PSEN1ΔE9 mice compared to age-matched wild-type mice, and that these cells are increased in transgenic mice by the treatment with ANDRO.

ANDRO does not affect neuronal differentiation in the dentate gyrus of APPswe/PSEN1ΔE9 mice. The increase in DCX+ cells in the dentate gyrus of APPswe/PSEN1ΔE9 mice treated with ANDRO might be mediated by the increased proliferation of neural precursor cells, and also by an increased differentiation of newborn cells into neurons. To assess neuronal differentiation of newborn cells DCX staining was

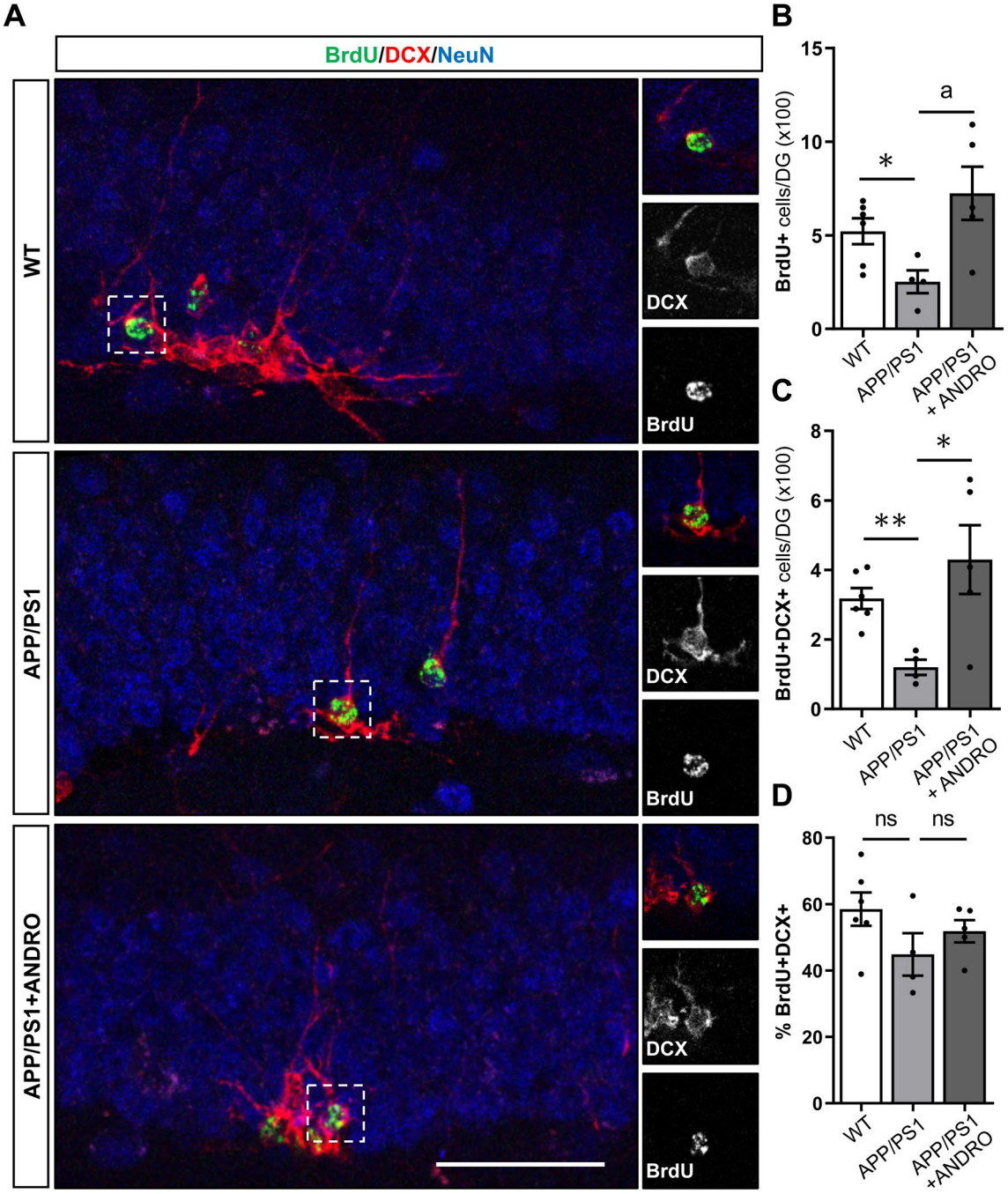

Figure 3. ANDRO does not affect neuronal differentiation in the dentate gyrus of APPswe/PSEN1ΔE9 mice. (**A**) Representative immunofluorescence staining of BrdU, and the neuronal markers DCX and NeuN in control wild-type (WT), APPswe/PSEN1ΔE9 (APP/PS1) mice, and APP/PS1 mice treated with ANDRO. Images correspond to maximal projection of 8 µm z-stack. Right panels show higher magnifications of single z-stack of dotted squares shown in left panels showing BrdU+DCX+ cells. Scale Bar: 50 µm. (**B**–**D**) Quantification of the total number of BrdU+ (**B**) and BrdU+DCX+ (**C**) cells in the GCL, and the percentage of BrdU+ cells expressing DCX (%BrdU+DCX+) (**D**), in animals treated with vehicle or ANDRO. Data are presented as mean ± SEM; WT = 6 mice; APP/PS1 = 4 mice; APP/PS1 + ANDRO = 5 mice. *p = 0.0255, [a]p = 0.0272 (**B**); *p = 0.0298, **p = 0.0014 (**C**); ns, non-significantly different, unpaired Student's t-test.

evaluated in BrdU+ cells (Fig. 3A) 14 days after BrdU injection (Fig. 1A, b). Reduced number of BrdU+ cells was determined in the dentate gyrus of APPswe/PSEN1ΔE9 compared with wild-type mice, and in agreement with the proliferation analysis (Fig. 1C), a significant increase in total number of BrdU+ cells was observed in APPswe/PSEN1ΔE9 treated with ANDRO (Fig. 3B). Similar results were observed for total number of cells positive for BrdU and DCX (BrdU+DCX+, Fig. 3C), supporting that neurogenesis is reduced in APPswe/PSEN1ΔE9 compared to wild-type mice and that ANDRO stimulates this process in AD mice.

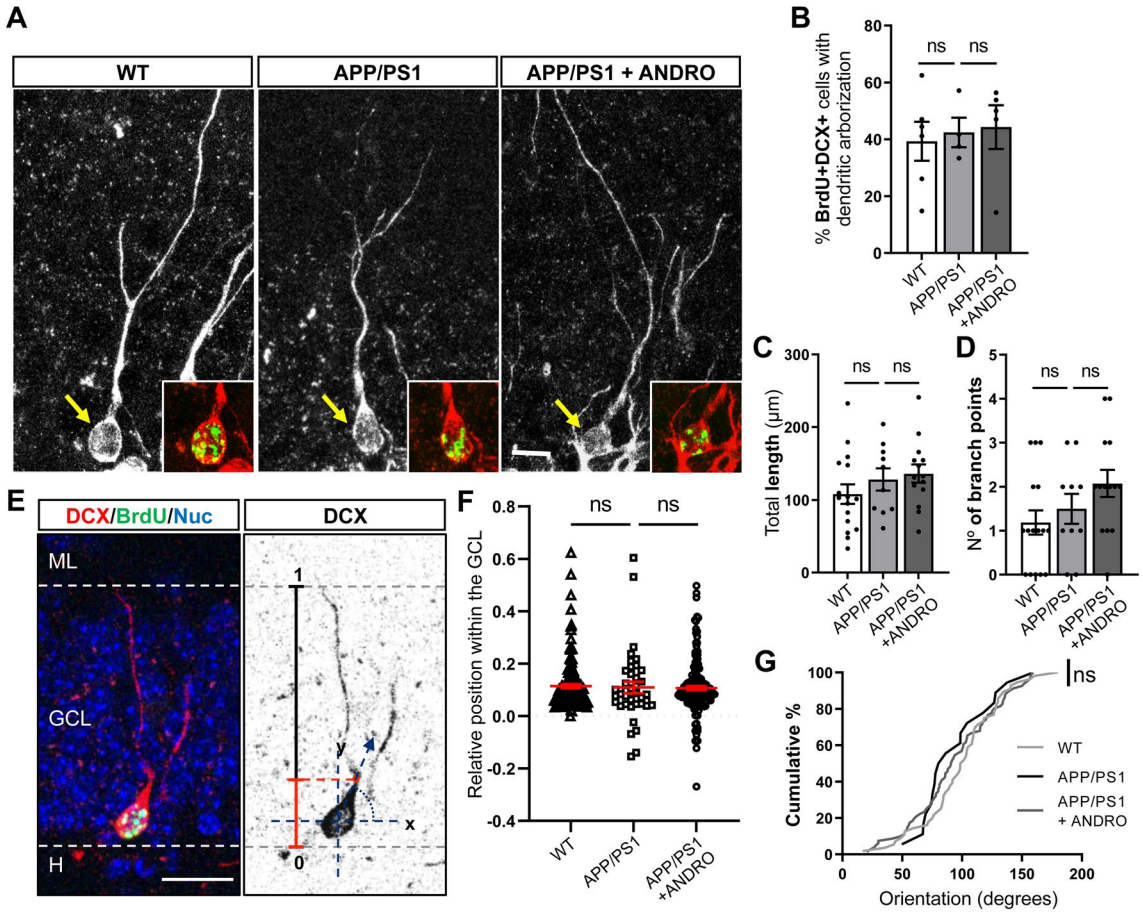

Figure 4. ANDRO does not affect early morphological development of newborn neurons. (**A**) Representative confocal images of BrdU+DCX+ cells showing dendritic arborization into the GCL towards the molecular layer in control wild-type (WT), APPswe/PSEN1ΔE9 (APP/PS1) mice, and APP/PS1 mice treated with ANDRO. Images correspond to maximal projection of 10 µm z-stack. Insets show z-stack of BrdU+DCX+ staining in cells indicated with the arrows (DCX: red; BrdU: green). Scale Bar: 10 µm (**B**) Quantification of the percentage of BrdU+DCX+ cells extending dendrites toward the molecular layer in WT, APP/PS1 mice and APP/PS1 mice treated with ANDRO. Data are presented as mean ± SEM; WT = 6 mice; APP/PS1 = 4 mice; APP/PS1 + ANDRO = 5 mice. ns, non-significantly different; one-way ANOVA test followed by Bonferroni post-hoc test. (**C**,**D**) Quantification of the total dendritic length (**C**) and number of branch points (**D**) of BrdU+DCX+ cells in WT, APP/PS1 and APP/PS1 mice treated with ANDRO. Data are presented as mean ± SEM; WT = 16 cells (N = 3 mice); APP/PS1 = 10 cells (N = 3 mice); APP/PS1 + ANDRO = 14 cells (N = 3 mice). One-way ANOVA test followed by Bonferroni post-hoc test. ns, non-significant. (**E**) Representative immunofluorescence of BrdU+DCX+ cell (left panel) and inverted DCX immunostaining (right panel) showing the schematic model of the analysis to assess the relative position of BrdU+DCX+ cells within the GCL, and the angular orientation of the initiation site (red dot), with the x-axis parallel to the GCL (0°–180°), the y axis pointing toward the hilus or ML (90° and 270°), and the origin at the center of the soma. (**F**) Quantification of the relative position of BrdU+DCX+ cells within the GCL. ns, non-significant, Mann–Whitney test. (**G**) Cumulative distribution plots of the angular orientation of the initiation site of BrdU+DCX+ cells. ns, non-significant, Kolmogorov–Smirnov test. (**D**,**E**): WT = 6 animals; APP/PS1 = 4 animals; APP/PS1 + ANDRO = 5 animals, N > 40 cells.

When assessing the percentage of BrdU+ cells expressing DCX, no differences were observed between wild-type mice, APPswe/PSEN1ΔE9 mice and APPswe/PSEN1ΔE9 mice treated with ANDRO (Fig. 3D), suggesting that ANDRO had no effect on neuronal differentiation.

These results suggest that the positive effect of ANDRO on neurogenesis in APPswe/PSEN1ΔE9 mice is not mediated by increased differentiation of neural precursor cells.

ANDRO does not affect early morphological development or migration of newborn neurons. To assess whether ANDRO modulates the development of newborn neurons, we evaluated the dendritic arborization in BrdU+DCX+ cells (Fig. 4A). This analysis was carried out in cells positive for BrdU to compare immature neurons of the same age (Fig. 1A, b), some of which extended dendrites into the GCL towards the molecular layer (Fig. 4A) or showed tangential processes in the SGZ. No changes in the percent-

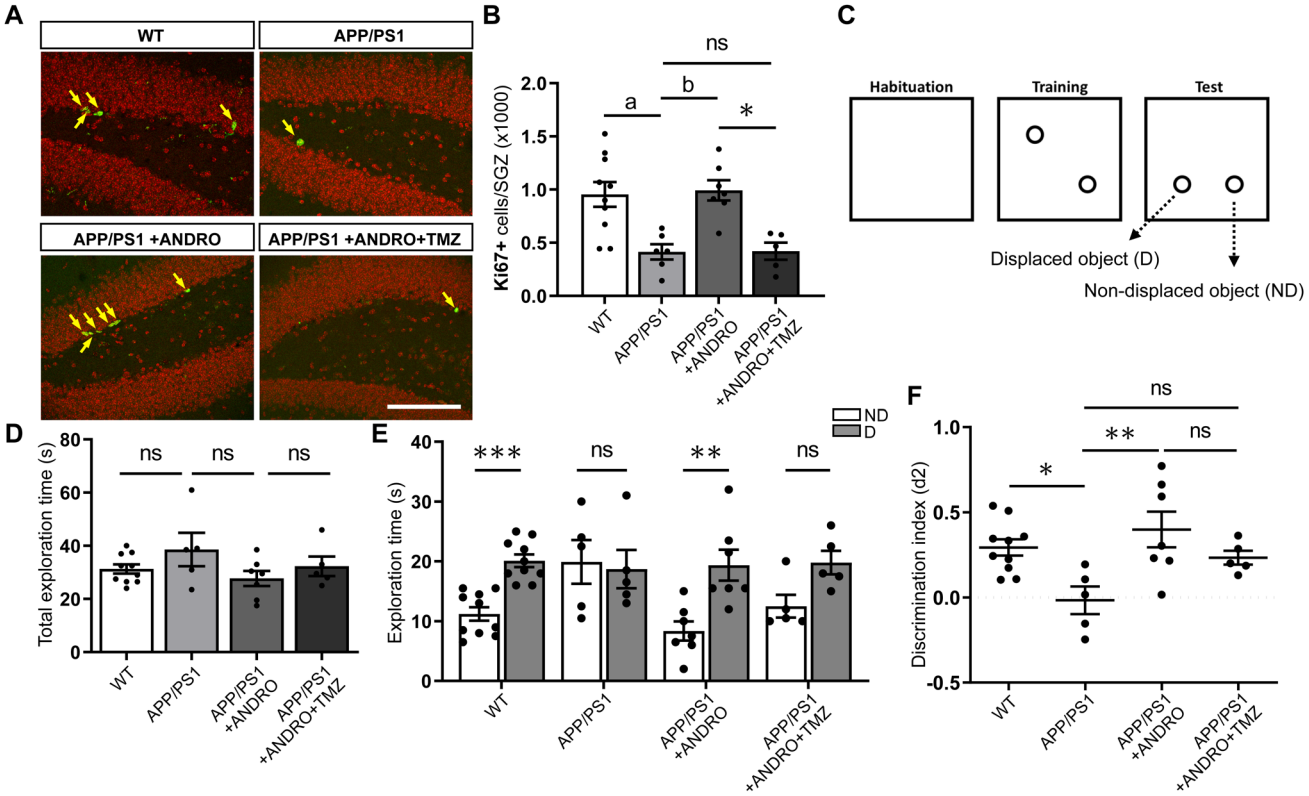

Figure 5. ANDRO improves spatial memory in APPswe/PSEN1ΔE9 mice. (**A**) Representative confocal images of the immunofluorescence of Ki67-positive (Ki67+, arrows) cells in the dentate gyrus of control wild-type (WT) mice, APPswe/PSEN1ΔE9 (APP/PS1) mice injected with vehicle, ANDRO or ANDRO + TMZ. Images correspond to maximal projection of 10 µm z-stack. Scale Bar: 50 µm. (**B**) Quantification of the total number of Ki67+ cells in the SGZ. One-way ANOVA test followed by Bonferroni post-hoc test. $^{a}p = 0.0185$; $^{b}p = 0.0177$; $^{*}p = 0.0139$. ns, non-significant. (**C**) Schematic representation of the object location memory (OLM) test. (**D**) Quantification of the total exploration time in WT mice, APP/PS1 mice injected with vehicle, ANDRO or ANDRO + TMZ. ns, non-significant, One-way ANOVA test followed by Bonferroni post-hoc test. (**E**) Quantification of the time spent exploring the non-displaced (ND) and displaced (D) objects. $^{***}p = 0.0002$, $^{**}p = 0.0012$, ns, non-significant. Mann–Whitney test. (**F**) Discrimination index (d2) calculated by dividing the difference of time spent to explore D and ND objects by the total time exploring both objects. $^{*}p = 0.0335$, $^{**}p = 0.0067$; ns, non-significantly different, one-way ANOVA test followed by Bonferroni post-hoc test. In (**B**–**F**), WT = 10 animals; APP/PS1 = 5 animals; APP/PS1 + ANDRO = 7 animals; APP/PS1 + ANDRO + TMZ = 5 animals.

age of BrdU+ DCX+ extending dendrites into the GCL were observed between the three experimental groups (Fig. 4B). Of these branched neurons, no changes were observed in total dendritic length (Fig. 4C) or in the number of branch points (Fig. 4D).

We evaluated the migration of BrdU+DCX+ cells into the GCL (Fig. 4E). Although in APPswe/PSEN1ΔE9 mice more cells were observed in the hilus (relative position < 0), no significant differences were observed between wild-type and APPswe/PSEN1ΔE9 mice, or between APPswe/PSEN1ΔE9 mice treated with ANDRO or vehicle (Fig. 4F), being most of the cells located in the inner third of the GCL as previously reported for adult-born neurons[39]. Finally, the orientation of the primary dendrite of BrdU+DCX+ cells showing arborization was evaluated (Fig. 4E). No changes were observed in the orientation between the three experimental groups (Fig. 4G).

Altogether, the data suggest that treatment with ANDRO did not induce global changes in early morphological development of adult-born neurons.

ANDRO improves spatial memory in APPswe/PSEN1ΔE9 mice. To evaluate the effect of ANDRO on spatial memory we used the OLM task, a hippocampal-dependent task that involves exploiting the innate tendency of mice to explore novel items, and is inherently not stressful[40]. For this experiment, 8-month-old APPswe/PSEN1ΔE9 mice were injected i.p. with 2 mg kg^{-1} ANDRO or vehicle solution 3 times a week for 4 weeks. Also, a group of 8-month-old non-transgenic wild-type littermates mice received vehicle injections 3 times a week for 4 weeks. To assess the potential role of newborn cells in the cognitive effect of ANDRO, a group of APPswe/PSEN1ΔE9 animals were injected with ANDRO plus the DNA-alkylating agent TMZ (25 mg kg^{-1}) that arrest cell proliferation and induces apoptosis of proliferating cells[41,42]. TMZ is able to cross the blood brain barrier[43,44], and inhibits proliferation of NPCs in the hippocampus[45]. TMZ was administered together with ANDRO aiming to prevent the proliferative effect of ANDRO on APPswe/PSEN1ΔE9 mice (Fig. 5A,B).

The OLM task consisted of a context habituation day (empty training arena), a training day with two objects, and a testing day in which one object was moved to a novel location (displaced object, D) while the other object was not moved (non-displaced object, ND) (Fig. 5C). No significant differences were observed between the four experimental groups in total exploration time (time spent exploring both objects) during the 5 min testing session (Fig. 5D). When evaluating exploration time per object, wild-type mice preferentially explored the displaced object compared to the non-displaced object, suggesting that animals remembered the original training experience (Fig. 5E). On the other hand, APPswe/PSEN1ΔE9 mice similarly explored both objects indicating no preference for the displaced object, in agreement with previous studies demonstrating a spatial memory deficit in this mouse model of AD[46–48]. APPswe/PSEN1ΔE9 mice treated with ANDRO spent significantly more time exploring the displaced object, suggesting an improved performance in the OLM task. Although in animals co-injected with ANDRO plus TMZ no statistical differences were observed between the time exploring the displaced versus the non-displaced object, these animals showed a preference for the displaced object (Fig. 5E). When evaluating the discrimination index, statistical differences were observed between wild-type and APPswe/PSEN1ΔE9 mice, which showed equal preference for the two objects (Fig. 5F). A significant increase was observed for APPswe/PSEN1ΔE9 mice treated with ANDRO compared to control APPswe/PSEN1ΔE9 mice. Although mice treated with ANDRO plus TMZ showed a positive value for the discrimination index, this was not statistically different from the discrimination index of control APPswe/PSEN1ΔE9, or APPswe/PSEN1ΔE9 + ANDRO mice (Fig. 5F). This suggest that although mice treated with ANDRO + TMZ show preference for the displaced object, TMZ tends to reduce the effect of ANDRO.

Discussion

Previously we reported that ANDRO treatment for 4 weeks increased the number of cells positive for the mitotic marker Ki67, which was also demonstrated in the present study, and increased DCX staining in the hippocampus of the APPswe/PSEN1ΔE9 mouse model of AD[24]. This animal model shows reduced hippocampal neurogenesis[7,11], which was also observed in the present study when comparing newborn DCX+ cells in APPswe/PSEN1ΔE9 versus age-matched wild-type mice. Here we deepen in the effect of ANDRO on neurogenesis in APPswe/PSEN1ΔE9 mice by evaluating proliferation, neural precursor cells population, neuronal differentiation, newborn neurons development, and spatial memory.

First, by using the thymidine analog BrdU that is incorporated in the DNA of proliferating cells during DNA synthesis, we determined that ANDRO induced the number of proliferative cells in the dentate gyrus of APPswe/PSEN1ΔE9 mice. Therefore, by both strategies used, Ki67 staining and BrdU incorporation, the data strongly suggest that ANDRO induces cell proliferation in the hippocampus of APPswe/PSEN1ΔE9 mice. ANDRO treatment also increased the total number of type 2a/b neural progenitors, neuroblasts and newborn DCX+ cells in the dentate gyrus of AD mice, cell populations that were decreased in APPswe/PSEN1ΔE9 versus wild-type mice. Interestingly, no changes in type 1 cells were observed between the experimental groups, suggesting that neurogenesis impairment in AD mice and stimulation with ANDRO are not mediated by global changes in the NSC population. Additionally, ANDRO induced no changes in neuronal differentiation of newborn BrdU+ cells, suggesting that the observed increase in DCX+ cells is due to the effect in proliferation of neural precursor cells and not due to an increase in their differentiation. Intriguingly, we did not observe changes between wild-type and APPswe/PSEN1ΔE9 mice in the percentage of BrdU+ cells expressing DCX two-weeks after birth, suggesting that differentiation is not impaired in AD mice. However, we previously determined a reduced differentiation of newborn BrdU cells 24 h after the BrdU injection in APPswe/PSEN1ΔE9 mice[7], and other studies have also suggested impaired differentiation in AD[11,49]. One possibility for this discrepancy is that there might be an increased elimination of cells unable to undergo proper differentiation and maturation in APPswe/PSEN1ΔE9 mice, a process that normally occurs in the adult hippocampus[50]. If so, the percentage of newborn cells positive for DCX may be increased after 2 weeks because of the elimination of undifferentiated cells, which might result in a strong decrease in total density of newborn DCX+ neurons even though the percentage of BrdU+ DCX+ cells appears unaffected. In agreement with this idea, it has been shown in different models of AD that survival of NPCs is affected[51]. Further analysis, including comparing the survival of newborn cells in wild-type versus APPswe/PSEN1ΔE9 mice, will be necessary to fully elucidate the contribution of abnormal neuronal differentiation and cell death to the strong differences in the total number of DCX + cells in APPswe/PSEN1ΔE9 versus wild-type mice.

One potential mechanism involved in the effect of ANDRO may include the inhibition of GSK-3β[52], which in turn could stimulate neurogenesis through different mechanisms. GSK-3β inhibition might induce the Wnt/β-catenin signaling cascade. Accordingly, we previously determined that ANDRO treatment induced the activation of the Wnt/β-catenin signaling in the hippocampus of wild-type and APPswe/PSEN1ΔE9 mice[24,52]. Compelling evidence indicate that a downregulation of this signaling pathway is associated to the pathophysiology of AD[53–55], and evidence suggest an association between Wnt signaling impairment and reduced neurogenesis in aging and AD[56]. The Wnt/β-catenin signaling pathway is a key signaling mechanisms regulating neurogenesis in the adult hippocampus[57–60], e.g. it controls proliferation of NPCs through the expression of the Wnt target gene Cyclin D1[61]. Therefore, ANDRO might control proliferation through this Wnt-mediated mechanism. In addition, activation of Wnt signaling by different strategies was shown to reduce spatial memory impairment in APPswe/PSEN1ΔE9 mice[48,62], which suggests that cognitive improvements induced by ANDRO in our and other studies[30–33] might involve the activation of the Wnt signaling pathway.

In addition, inhibition of GSK-3β may have an impact on APP processing. GSK-3β plays a critical role in the development of the histopathological hallmarks of AD[63], including downregulation of non-amyloidogenic cleavage of APP[64]. Furthermore, GSK-3β inhibition reduces the putative β-secretase BACE1-mediated cleavage of APP[65]. Also, it has been suggested that inhibition of Wnt signaling promotes the amyloidogenic proteolytic

processing of APP, while Wnt signaling activation promotes the non-amyloidogenic processing of APP and reduces the levels of Aβ42 and its aggregates[66]. In accordance, ANDRO have shown to reduce Aβ levels and Aβ aggregates in animal models of AD[31,67]. In addition, in APPswe/PSEN1ΔE9 mice ANDRO affects the maturation of amyloid plaques[31]. Since Aβ deposition is linked to abnormal hippocampal neurogenesis[51,68], by inhibiting GSK-3β ANDRO may stimulate neurogenesis through reducing Aβ deposition.

ANDRO effects may also involve the activation of Akt signaling. ANDRO was shown to modulate this signaling in the hippocampus of a rat model of chronic cerebral hypoperfusion (CCH) characterized by increased neurodegeneration, neuroinflammation and apoptosis[25], as well as in neuroblastoma SH-SY5Y cells[69]. In CCH model, ANDRO treatment reduced the levels of the tumor suppressor PTEN and increased the levels of Akt. Akt modulates processes such as cell growth, proliferation, and survival[70]. In addition, stimulation of PI3K/Akt signaling enhances neurogenesis[71], while inhibition of this pathway prevents the induction of neurogenesis by physiological stimulation[72,73] which was associated to a reduced survival of newly generated neurons[72]. Therefore, through Akt signaling ANDRO might induce the survival of newborn neurons, which is affected in AD[51]. In support of this notion, based on BrdU incorporation assays, an estimated ~ 57% reduction in the number of BrdU + cells was observed in APPswe/PSEN1ΔE9 mice 14 days after BrdU administration (252 ± 61.4 cells, Fig. 2D) compared to 3 days after BrdU administration (586 ± 149.3 cells, Fig. 1C), while in APPswe/PSEN1ΔE9 mice treated with ANDRO, the estimated reduction in BrdU + cells was ~ 49% (3 dpi: 1426 ± 155.9 cells; 14 dpi: 725 ± 142.1). Therefore, ANDRO may induce proliferation and survival of NPC and immature neurons. We observed no changes in early morphological development of immature neurons, including dendritic arborization (total dendritic length and number of branch points) and angular orientation of dendrites, neither in migration of newborn neurons into the GCL. However, further analyses are needed to evaluate if ANDRO may stimulate maturation, integration and survival of adult-born neurons.

ANDRO might also restore neurogenesis in APPswe/PSEN1ΔE9 mice through its anti-inflammatory capacity. Neuroinflammation is considered a major feature of AD and other neurodegenerative diseases, a process including microglia and astrocyte activation, proinflammatory cytokines production and reactive oxygen species[74–76]. Increased microglia activity has been correlated with a decline in NSCs proliferation and neuronal differentiation and survival[77–79], while anti-inflammatory treatment restores neurogenesis in inflammatory conditions[78,80]. ANDRO has shown anti-inflammatory effects in different models of AD. In the rodent Octodon degus that has been proposed as a natural model for AD since it spontaneously develops neuropathological hallmarks of AD pathology[81–83], ANDRO reduced astrogliosis, oxidative stress and pro-inflammatory cytokines[67]. Also, treatment with nanoparticles loaded with ANDRO reduced astrocyte activation in TgCRND8 mouse model of AD[84]. In addition, ANDRO reduced the production of proinflammatory cytokines in Aβ-stimulated microglial cells[85], and reduced astrocyte activation and the expression of proinflammatory cytokines in a model of CCH[27]. Reports indicate that ANDRO ameliorate inflammation by inhibiting the activation of nuclear factor-κB (NF-κB)[26,85], which was identified as a critical mediator of stress-induced neurogenesis impairment[86]. Interestingly, the enzyme GSK-3β has the capacity to positively regulate NF-κB[87], while the Wnt/β-catenin signaling pathway inactivates the transcriptional activity of NF-κB[88,89]. Therefore, ANDRO may reduce inflammation and promote neurogenesis through a mechanism involving the inhibition of GSK-3β and consequent activation of Wnt signaling.

We determined that ANDRO improved the performance of APPswe/PSEN1ΔE9 mice in the OLM task, which have shown to be dependent on the hippocampus for encoding, consolidation and retrieval[40]. This result is in agreement with previous studies showing that ANDRO improved the performance of animal models of AD in different spatial memory tasks[30–33,84]. It has been shown that altered hippocampal neurogenesis contributes to the learning and memory deficits in AD[90], and increasing neurogenesis promotes cognitive performance in AD mice[91]. Although, co-treatment with the antimitotic drug TMZ tends to reduce the effect of ANDRO, it did not significantly prevent cognitive improvement. Of note, although TMZ treatment reduced the number of Ki67-positive cells, the decrease of DCX-positive neurons was not statistically significant (Supplementary Fig. 1), likely due to the high variability observed in the number of DCX cells in animals treated with the drug. Still, these results suggests that other effects of ANDRO in addition to the increase in neurogenesis (e.g. decrease in Aβ burden[31]), might underlie the observed cognitive improvement. In this context, it was showed in 5xFAD mice that increasing neurogenesis through genetic or pharmacologic methods alone results in slight cognitive enhancement, and full rescue requires also increasing brain derived neurotrophic factor (BDNF) levels[92]. Importantly, ANDRO has shown to induce BDNF levels in the hippocampus[27], which may also contribute to the cognitive improvements of ANDRO in APPswe/PSEN1ΔE9 mice.

In summary, our results indicate that ANDRO stimulates neurogenesis in the hippocampus of APPswe/PSEN1ΔE9 by inducing proliferation of neural precursor cells. Although inhibition of proliferation tends to decrease the improvement in spatial memory performance induced by ANDRO, further analysis with genetic manipulation of neurogenesis in animals treated with ANDRO will provide more substantial evidence to support the contribution of newborn neurons to the cognitive effects. Altogether, our findings support that ANDRO is a natural product with potential therapeutic benefits for the treatment of brain conditions affecting neurogenesis and cognition.

Materials and methods

Animals and treatments. All experimental procedures involving mice were conducted in accordance with NIH and ARRIVE guidelines and were approved by the Bioethical Committee of Universidad Andrés Bello. Female APPswe/PSEN1ΔE9 (stock #004462, The Jackson Laboratory) and non-transgenic wild-type littermates were used for the experiments. Mice had access to water and food ad libitum in a 12:12 h light/dark cycle. At 8 month of age mice were injected i.p. with 2 mg kg^{-1} ANDRO (Sigma-Aldrich) or vehicle (DMSO, Sigma-Aldrich), 3 times a week for 4 weeks. Some animals received a daily i.p. injection of 100 mg kg^{-1} 5-Bromo-

2′-deoxyuridine (BrdU, Sigma-Aldrich) for the last 3 days of ANDRO/vehicle treatment and were sacrificed 24 h after the last BrdU injection. Other group receive daily i.p. injection of 100 mg kg^{-1} BrdU for 3 consecutive days at 2 weeks of ANDRO/vehicle treatment and were sacrificed 2 weeks later. Eight-month-old mice used for behavioral testing were injected i.p. with 2 mg kg^{-1} ANDRO or vehicle 3 times a week for 4 weeks. Some animals were co-injected i.p. with 2 mg kg^{-1} ANDRO plus 25 mg kg^{-1} temozolomide (TMZ, AK Scientific, Inc) 3 times a week for 4 weeks.

Perfusion, postfixation and tissue sectioning. Animals were anesthetized with a mixture of ketamine/xylazine (200 mg/kg, 20 mg/kg), and transcardially perfused with 50 ml ice-cold 0.9% NaCl, followed by 50 ml ice-cold 4% paraformaldehyde (PFA, Sigma-Aldrich/Merck Group) in 0.115 M NaH_2PO_4. Brains were removed and post-fixed in 4% PFA in PBS for 24 h at room temperature and then dehydrated in 30% sucrose. Brains were sectioned on a cryostat (Leica Microsystems) and collected in ice-cold-PBS in multiwell dishes as previously described[7]. Tissue sections were sequentially collected in 12 sets of serial slices of 50 µm. Each set contained 5–7 tissue sections covering the entire length of the hippocampus.

Immunohistochemistry. Free-floating sections were washed three times in 0.15% Triton X-100 in PBS, and then incubated with 0.3% H_2O_2 for 30 min at room temperature. After washing three times in 0.15% Triton X-100 in PBS for 5 min, samples were incubated for 1 h with blocking solution (PBS, 5% BSA, 0.15% Triton X-100), and then incubated overnight at 4 °C with rabbit anti-DCX (4604S, Cell Signaling Technology Inc Danvers) diluted 1:400 in blocking solution. After washing, sections were incubated with biotinylated donkey anti-rabbit secondary antibody (1:250, BA-1000, Vector laboratories) for 1 h, washed in 0.15% Triton X-100 in PBS, and then incubated with avidin–biotin–peroxidase complex (1:125, Vectastain ABC Elite kit, PK-6101, Vector laboratories) for 1 h. Finally, sections were incubated with 0.3% H_2O_2 and 0.5 mg ml^{-1} 3,3-diaminobenzidine (DAB, Sigma) in Tris–HCL 50 mM (ph 7.6). Slides were washed, dehydrated, and coverslipped using Entellan® (Merck Millipore). For in vivo analysis images were acquire in MOTIC® (BA310, light microscope). For the analysis of total number of DCX+ cells, all tissues of 1–2 sets of the serial slices (see tissue sectioning) were acquired for each animal. Total number of cells counted in one set were multiplied by the total number of sets to obtain an estimation of the total number of DCX+ cells in the whole dentate gyrus.

Immunofluorescence. Immunodetection of proliferation, progenitor and neuronal markers, and BrdU was carried out as previously described[7,93]. Primary antibodies used were rabbit anti-DCX (1:750, Cell Signaling Technology Inc.), goat anti-DCX (1:250, Santa Cruz Biotechnology), rabbit anti-Ki67 (1:250, Abcam), mouse anti-NeuN (1:300, Millipore), mouse anti-GFAP (1:8000, Sigma), goat anti-Sox2 (1:2000, R&D Systems), rat anti-BrdU (1:300, Abcam). As secondary antibodies Alexa (1:500, Molecular Probes) and DyLight (1:500, Abcam) conjugated antibodies were used. NucBlue (Life Technologies) was used as nuclear dye. Slices were mounted on gelatin-coated slides with Fluoromont-G (Electron Microscopy Sciences).

Proliferation, differentiation, and morphological analyses. For proliferation, BrdU and Ki67-positive cells were counted in 1–2 sets of tissue sections (see tissue sectioning) using a fluorescence microscope (Nikon Eclipse Ti), and the number of cells was multiplied by the total number of tissues sets. For the analyses of neural precursor cells and neuroblasts, differentiation and migration, images were acquired by confocal laser microscopy (Leica TCS SP8 microscope), with a 40X objective and a z-axis interval of 1 µm. z-projections were made with ImageJ software (NIH). To analyze neural precursor cells and neuroblasts, all tissues in one set of tissue sections were analyzed for GFAP, Sox2 and DCX staining, and the number of cells counted was multiplied by the total number of sets. For differentiation analysis, all BrdU-positive cells in one set of tissue sections were analyzed for DCX staining. For morphological analysis, BrdU+DCX+ cells were acquired with a 60X objective by confocal laser microscopy (Leica TCS SP8 microscope) using 40–50 z-axis interval of 0.5 µm. Analysis of total dendritic length, and number of branch points were made using the Simple Neurite tracer plugin using FIJI software[94]. Angular orientation and position of newborn neurons within the GCL was evaluated as described previously[95,96] in all BrdU+DCX+ cells of one set of tissue sections.

Object location memory (OLM) test. The OLM test was performed as previously described[97] with some modifications[98]. Briefly, animals were habituated for 5 min in an apparatus that contained a cage inside an insonorized chamber. During the training session, the cage contained two identical objects placed in opposite quadrants of the chamber; animals were placed in the center of the cage and left to explore for 5 min. In the test session, one object was moved to a different position (displaced object, D), while the other object was not moved (none-displaced, ND); animals were left to explore for 5 min. The exploration time was recorded and defined as time spent sniffing or touching the object with the nose and/or forepaws. Total exploration time indicates the time spent exploring both objects (D + ND). Animals that did not explore a total of 15 s for both objects during the testing session were excluded from the analysis. The discrimination index was calculated by dividing the difference of time spent to explore D and ND objects by the total time exploring both objects [discrimination index: (time D − time ND)/(time D + time ND)]. Timing and video analysis was conducted by an experimenter blind to the experimental conditions.

Statistical analysis. All statistical analyses were performed using Prism Software 9 (GraphPad Software, LLC). All data were checked for normality using Shapiro–Wilk test. For data with normal distribution to compare mean values between two groups a two-tailed unpaired Student's *t*-test was used with a significance level set

to $\alpha = 0.05$. For comparison between more than two groups, one-way ANOVA followed by Bonferroni multiple comparison post-hoc test was used to determine statistical significance. For data with non-normal distribution two-tailed Mann–Whitney test was used to compare mean values between two groups. For cumulative distribution of dendritic initiation site, the Kolmogorov–Smirnov (K–S) test was used. In all graphs the data represent the mean ± SEM. Number of animals per experimental group, or number of neurons analyzed in each experiment, is indicated in each Figure legend. $p < 0.05$ was considered statistically significant.

Data availability

The datasets generated during and/or analyzed during the current study are available from the corresponding author on reasonable request.

Received: 13 May 2021; Accepted: 8 November 2021
Published online: 25 November 2021

References

1. Haque, R. U. & Levey, A. I. Alzheimer's disease: A clinical perspective and future nonhuman primate research opportunities. *Proc. Natl. Acad. Sci. U. S. A.* https://doi.org/10.1073/pnas.1912954116 (2019).
2. Serrano-Pozo, A., Frosch, M. P., Masliah, E. & Hyman, B. T. Neuropathological alterations in Alzheimer disease. *Cold Spring Harb. Perspect. Med.* **1**, a006189. https://doi.org/10.1101/cshperspect.a006189 (2011).
3. Selkoe, D. J. & Hardy, J. The amyloid hypothesis of Alzheimer's disease at 25 years. *EMBO Mol. Med.* **8**, 595–608. https://doi.org/10.15252/emmm.201606210 (2016).
4. Moreno-Jimenez, E. P. *et al.* Adult hippocampal neurogenesis is abundant in neurologically healthy subjects and drops sharply in patients with Alzheimer's disease. *Nat. Med.* **25**, 554–560. https://doi.org/10.1038/s41591-019-0375-9 (2019).
5. Tobin, M. K. *et al.* Human hippocampal neurogenesis persists in aged adults and Alzheimer's disease patients. *Cell Stem Cell* **24**, 974-982 e973. https://doi.org/10.1016/j.stem.2019.05.003 (2019).
6. Ekonomou, A. *et al.* Stage-specific changes in neurogenic and glial markers in Alzheimer's disease. *Biol. Psychiatry* **77**, 711–719. https://doi.org/10.1016/j.biopsych.2014.05.021 (2015).
7. Abbott, A. C., Calderon Toledo, C., Aranguiz, F. C., Inestrosa, N. C. & Varela-Nallar, L. Tetrahydrohyperforin increases adult hippocampal neurogenesis in wild-type and APPswe/PS1DeltaE9 mice. *J. Alzheimers Dis.* **34**, 873–885. https://doi.org/10.3233/JAD-121714 (2013).
8. Hamilton, L. K. *et al.* Widespread deficits in adult neurogenesis precede plaque and tangle formation in the 3xTg mouse model of Alzheimer's disease. *Eur. J. Neurosci.* **32**, 905–920. https://doi.org/10.1111/j.1460-9568.2010.07379.x (2010).
9. Zeng, Q., Zheng, M., Zhang, T. & He, G. Hippocampal neurogenesis in the APP/PS1/nestin-GFP triple transgenic mouse model of Alzheimer's disease. *Neuroscience* **314**, 64–74. https://doi.org/10.1016/j.neuroscience.2015.11.054 (2016).
10. Moon, M., Cha, M. Y. & Mook-Jung, I. Impaired hippocampal neurogenesis and its enhancement with ghrelin in 5XFAD mice. *J. Alzheimers Dis.* **41**, 233–241. https://doi.org/10.3233/JAD-132417 (2014).
11. Demars, M., Hu, Y. S., Gadadhar, A. & Lazarov, O. Impaired neurogenesis is an early event in the etiology of familial Alzheimer's disease in transgenic mice. *J. Neurosci. Res.* **88**, 2103–2117. https://doi.org/10.1002/jnr.22387 (2010).
12. Fiorentini, A., Rosi, M. C., Grossi, C., Luccarini, I. & Casamenti, F. Lithium improves hippocampal neurogenesis, neuropathology and cognitive functions in APP mutant mice. *PLoS One* **5**, e14382. https://doi.org/10.1371/journal.pone.0014382 (2010).
13. van Praag, H. *et al.* Functional neurogenesis in the adult hippocampus. *Nature* **415**, 1030–1034. https://doi.org/10.1038/4151030a (2002).
14. Ge, S. *et al.* GABA regulates synaptic integration of newly generated neurons in the adult brain. *Nature* **439**, 589–593. https://doi.org/10.1038/nature04404 (2006).
15. Toni, N. & Schinder, A. F. Maturation and functional integration of new granule cells into the adult hippocampus. *Cold Spring Harb. Perspect. Biol.* **8**, a018903. https://doi.org/10.1101/cshperspect.a018903 (2015).
16. Snyder, J. S., Kee, N. & Wojtowicz, J. M. Effects of adult neurogenesis on synaptic plasticity in the rat dentate gyrus. *J. Neurophysiol.* **85**, 2423–2431. https://doi.org/10.1152/jn.2001.85.6.2423 (2001).
17. Lacefield, C. O., Itskov, V., Reardon, T., Hen, R. & Gordon, J. A. Effects of adult-generated granule cells on coordinated network activity in the dentate gyrus. *Hippocampus* **22**, 106–116. https://doi.org/10.1002/hipo.20860 (2012).
18. Marin-Burgin, A., Mongiat, L. A., Pardi, M. B. & Schinder, A. F. Unique processing during a period of high excitation/inhibition balance in adult-born neurons. *Science* **335**, 1238–1242. https://doi.org/10.1126/science.1214956 (2012).
19. Drew, L. J. *et al.* Activation of local inhibitory circuits in the dentate gyrus by adult-born neurons. *Hippocampus* **26**, 763–778. https://doi.org/10.1002/hipo.22557 (2016).
20. Deng, W., Aimone, J. B. & Gage, F. H. New neurons and new memories: How does adult hippocampal neurogenesis affect learning and memory?. *Nat. Rev. Neurosci.* **11**, 339–350. https://doi.org/10.1038/nrn2822 (2010).
21. Aimone, J. B., Deng, W. & Gage, F. H. Resolving new memories: A critical look at the dentate gyrus, adult neurogenesis, and pattern separation. *Neuron* **70**, 589–596. https://doi.org/10.1016/j.neuron.2011.05.010 (2011).
22. Anacker, C. & Hen, R. Adult hippocampal neurogenesis and cognitive flexibility—Linking memory and mood. *Nat. Rev. Neurosci.* **18**, 335–346. https://doi.org/10.1038/nrn.2017.45 (2017).
23. Sareer, O., Ahmad, S. & Umar, S. Andrographis paniculata: A critical appraisal of extraction, isolation and quantification of andrographolide and other active constituents. *Nat. Prod. Res.* **28**, 2081–2101. https://doi.org/10.1080/14786419.2014.924004 (2014).
24. Varela-Nallar, L., Arredondo, S. B., Tapia-Rojas, C., Hancke, J. & Inestrosa, N. C. Andrographolide stimulates neurogenesis in the adult hippocampus. *Neural Plast.* **2015**, 935403. https://doi.org/10.1155/2015/935403 (2015).
25. Wang, D. P. *et al.* Neuroprotective effects of andrographolide on chronic cerebral hypoperfusion-induced hippocampal neuronal damage in rats possibly via PTEN/AKT signaling pathway. *Acta Histochem.* **122**, 151514. https://doi.org/10.1016/j.acthis.2020.151514 (2020).
26. Tao, L. *et al.* Andrographolide alleviates acute brain injury in a rat model of traumatic brain injury: Possible involvement of inflammatory signaling. *Front. Neurosci.* **12**, 657. https://doi.org/10.3389/fnins.2018.00657 (2018).
27. Wang, D. P. *et al.* Andrographolide enhances hippocampal BDNF signaling and suppresses neuronal apoptosis, astroglial activation, neuroinflammation, and spatial memory deficits in a rat model of chronic cerebral hypoperfusion. *Naunyn Schmiedebergs Arch. Pharmacol.* **392**, 1277–1284. https://doi.org/10.1007/s00210-019-01672-9 (2019).
28. Ahmed, S., Kwatra, M., Ranjan Panda, S., Murty, U. S. N. & Naidu, V. G. M. Andrographolide suppresses NLRP3 inflammasome activation in microglia through induction of parkin-mediated mitophagy in in-vitro and in-vivo models of Parkinson disease. *Brain Behav. Immun.* **91**, 142–158. https://doi.org/10.1016/j.bbi.2020.09.017 (2021).
29. Geng, J. *et al.* Andrographolide alleviates Parkinsonism in MPTP-PD mice via targeting mitochondrial fission mediated by dynamin-related protein 1. *Br. J. Pharmacol.* **176**, 4574–4591. https://doi.org/10.1111/bph.14823 (2019).

30. Geng, J. *et al.* Andrographolide sulfonate improves Alzheimer-associated phenotypes and mitochondrial dysfunction in APP/PS1 transgenic mice. *Biomed. Pharmacother.* **97**, 1032–1039. https://doi.org/10.1016/j.biopha.2017.11.039 (2018).
31. Serrano, F. G. *et al.* Andrographolide reduces cognitive impairment in young and mature AbetaPPswe/PS-1 mice. *Mol. Neurodegener.* **9**, 61. https://doi.org/10.1186/1750-1326-9-61 (2014).
32. Cisternas, P., Oliva, C. A., Torres, V. I., Barrera, D. P. & Inestrosa, N. C. Presymptomatic treatment with andrographolide improves brain metabolic markers and cognitive behavior in a model of early-onset Alzheimer's disease. *Front. Cell Neurosci.* **13**, 295. https://doi.org/10.3389/fncel.2019.00295 (2019).
33. Rivera, D. S. *et al.* Andrographolide recovers cognitive impairment in a natural model of Alzheimer's disease (*Octodon degus*). *Neurobiol. Aging* **46**, 204–220. https://doi.org/10.1016/j.neurobiolaging.2016.06.021 (2016).
34. Garcia-Alloza, M. *et al.* Characterization of amyloid deposition in the APPswe/PS1dE9 mouse model of Alzheimer disease. *Neurobiol. Dis.* **24**, 516–524. https://doi.org/10.1016/j.nbd.2006.08.017 (2006).
35. Brown, J. P. *et al.* Transient expression of doublecortin during adult neurogenesis. *J. Comp. Neurol.* **467**, 1–10. https://doi.org/10.1002/cne.10874 (2003).
36. Seri, B., Garcia-Verdugo, J. M., McEwen, B. S. & Alvarez-Buylla, A. Astrocytes give rise to new neurons in the adult mammalian hippocampus. *J. Neurosci.* **21**, 7153–7160 (2001).
37. Zhao, C., Deng, W. & Gage, F. H. Mechanisms and functional implications of adult neurogenesis. *Cell* **132**, 645–660. https://doi.org/10.1016/j.cell.2008.01.033 (2008).
38. Kempermann, G., Jessberger, S., Steiner, B. & Kronenberg, G. Milestones of neuronal development in the adult hippocampus. *Trends Neurosci.* **27**, 447–452. https://doi.org/10.1016/j.tins.2004.05.013 (2004).
39. Kempermann, G., Gast, D., Kronenberg, G., Yamaguchi, M. & Gage, F. H. Early determination and long-term persistence of adult-generated new neurons in the hippocampus of mice. *Development* **130**, 391–399. https://doi.org/10.1242/dev.00203 (2003).
40. Vogel-Ciernia, A. & Wood, M. A. Examining object location and object recognition memory in mice. *Curr. Protoc. Neurosci.* **69**, 8–31. https://doi.org/10.1002/0471142301.ns0831s69 (2014).
41. Crespo, I. *et al.* Molecular and genomic alterations in glioblastoma multiforme. *Am. J. Pathol.* **185**, 1820–1833. https://doi.org/10.1016/j.ajpath.2015.02.023 (2015).
42. Zhang, J., Stevens, M. F. & Bradshaw, T. D. Temozolomide: Mechanisms of action, repair and resistance. *Curr. Mol. Pharmacol.* **5**, 102–114. https://doi.org/10.2174/1874467211205010102 (2012).
43. Agarwala, S. S. & Kirkwood, J. M. Temozolomide, a novel alkylating agent with activity in the central nervous system, may improve the treatment of advanced metastatic melanoma. *Oncologist* **5**, 144–151. https://doi.org/10.1634/theoncologist.5-2-144 (2000).
44. Patel, M., McCully, C., Godwin, K. & Balis, F. M. Plasma and cerebrospinal fluid pharmacokinetics of intravenous temozolomide in non-human primates. *J. Neurooncol.* **61**, 203–207. https://doi.org/10.1023/a:1022592913323 (2003).
45. Garthe, A., Behr, J. & Kempermann, G. Adult-generated hippocampal neurons allow the flexible use of spatially precise learning strategies. *PLoS One* **4**, e5464. https://doi.org/10.1371/journal.pone.0005464 (2009).
46. Reiserer, R. S., Harrison, F. E., Syverud, D. C. & McDonald, M. P. Impaired spatial learning in the APPSwe + PSEN1DeltaE9 bigenic mouse model of Alzheimer's disease. *Genes Brain Behav.* **6**, 54–65. https://doi.org/10.1111/j.1601-183X.2006.00221.x (2007).
47. Frye, C. A. & Walf, A. A. Effects of progesterone administration and APPswe+PSEN1Deltae9 mutation for cognitive performance of mid-aged mice. *Neurobiol. Learn. Mem.* **89**, 17–26. https://doi.org/10.1016/j.nlm.2007.09.008 (2008).
48. Toledo, E. M. & Inestrosa, N. C. Activation of Wnt signaling by lithium and rosiglitazone reduced spatial memory impairment and neurodegeneration in brains of an APPswe/PSEN1DeltaE9 mouse model of Alzheimer's disease. *Mol. Psychiatry* **15**(272–285), 228. https://doi.org/10.1038/mp.2009.72 (2010).
49. Wang, R., Dineley, K. T., Sweatt, J. D. & Zheng, H. Presenilin 1 familial Alzheimer's disease mutation leads to defective associative learning and impaired adult neurogenesis. *Neuroscience* **126**, 305–312. https://doi.org/10.1016/j.neuroscience.2004.03.048 (2004).
50. Sierra, A. *et al.* Microglia shape adult hippocampal neurogenesis through apoptosis-coupled phagocytosis. *Cell Stem Cell* **7**, 483–495. https://doi.org/10.1016/j.stem.2010.08.014 (2010).
51. Liu, H., Zhang, H. & Ma, Y. Molecular mechanisms of altered adult hippocampal neurogenesis in Alzheimer's disease. *Mech. Ageing Dev.* **195**, 111452. https://doi.org/10.1016/j.mad.2021.111452 (2021).
52. Tapia-Rojas, C. *et al.* Andrographolide activates the canonical Wnt signalling pathway by a mechanism that implicates the non-ATP competitive inhibition of GSK-3beta: Autoregulation of GSK-3beta in vivo. *Biochem. J.* **466**, 415–430. https://doi.org/10.1042/BJ20140207 (2015).
53. De Ferrari, G. V. & Inestrosa, N. C. Wnt signaling function in Alzheimer's disease. *Brain Res. Brain Res. Rev.* **33**, 1–12. https://doi.org/10.1016/s0165-0173(00)00021-7 (2000).
54. Oliva, C. A., Montecinos-Oliva, C. & Inestrosa, N. C. Wnt signaling in the central nervous system: New insights in health and disease. *Prog. Mol. Biol. Transl. Sci.* **153**, 81–130. https://doi.org/10.1016/bs.pmbts.2017.11.018 (2018).
55. Inestrosa, N. C. & Varela-Nallar, L. Wnt signaling in the nervous system and in Alzheimer's disease. *J. Mol. Cell Biol.* **6**, 64–74. https://doi.org/10.1093/jmcb/mjt051 (2014).
56. Arredondo, S. B., Valenzuela-Bezanilla, D., Mardones, M. D. & Varela-Nallar, L. Role of Wnt signaling in adult hippocampal neurogenesis in health and disease. *Front. Cell Dev. Biol.* **8**, 860. https://doi.org/10.3389/fcell.2020.00860 (2020).
57. Lie, D. C. *et al.* Wnt signalling regulates adult hippocampal neurogenesis. *Nature* **437**, 1370–1375. https://doi.org/10.1038/nature04108 (2005).
58. Kuwabara, T. *et al.* Wnt-mediated activation of NeuroD1 and retro-elements during adult neurogenesis. *Nat. Neurosci.* **12**, 1097–1105. https://doi.org/10.1038/nn.2360 (2009).
59. Mardones, M. D. *et al.* Frizzled-1 receptor regulates adult hippocampal neurogenesis. *Mol. Brain* **9**, 29. https://doi.org/10.1186/s13041-016-0209-3 (2016).
60. Varela-Nallar, L. & Inestrosa, N. C. Wnt signaling in the regulation of adult hippocampal neurogenesis. *Front. Cell Neurosci.* **7**, 100. https://doi.org/10.3389/fncel.2013.00100 (2013).
61. Qu, Q. *et al.* Wnt7a regulates multiple steps of neurogenesis. *Mol. Cell Biol.* **33**, 2551–2559. https://doi.org/10.1128/MCB.00325-13 (2013).
62. Vargas, J. Y., Fuenzalida, M. & Inestrosa, N. C. In vivo activation of Wnt signaling pathway enhances cognitive function of adult mice and reverses cognitive deficits in an Alzheimer's disease model. *J. Neurosci.* **34**, 2191–2202. https://doi.org/10.1523/JNEUROSCI.0862-13.2014 (2014).
63. Llorens-Martin, M., Jurado, J., Hernandez, F. & Avila, J. GSK-3beta, a pivotal kinase in Alzheimer disease. *Front. Mol. Neurosci.* **7**, 46. https://doi.org/10.3389/fnmol.2014.00046 (2014).
64. Zhang, H., Ma, Q., Zhang, Y. W. & Xu, H. Proteolytic processing of Alzheimer's beta-amyloid precursor protein. *J. Neurochem.* **120**(Suppl 1), 9–21. https://doi.org/10.1111/j.1471-4159.2011.07519.x (2012).
65. Ly, P. T. *et al.* Inhibition of GSK3beta-mediated BACE1 expression reduces Alzheimer-associated phenotypes. *J. Clin. Investig.* **123**, 224–235. https://doi.org/10.1172/JCI64516 (2013).
66. Tapia-Rojas, C., Burgos, P. V. & Inestrosa, N. C. Inhibition of Wnt signaling induces amyloidogenic processing of amyloid precursor protein and the production and aggregation of Amyloid-beta (Abeta)42 peptides. *J. Neurochem.* **139**, 1175–1191. https://doi.org/10.1111/jnc.13873 (2016).
67. Lindsay, C. B. *et al.* Andrographolide reduces neuroinflammation and oxidative stress in aged *Octodon degus*. *Mol. Neurobiol.* **57**, 1131–1145. https://doi.org/10.1007/s12035-019-01784-6 (2020).

68. Amber, S. *et al.* Amyloid-beta induced neurotoxicity impairs cognition and adult hippocampal neurogenesis in a mouse model for Alzheimer's disease. *Curr. Alzheimer Res.* **17**, 1033–1042. https://doi.org/10.2174/1567205017666201224162730 (2020).
69. Zhang, H., Wang, W. & Du, Q. Andrographolide attenuates bupivacaine-induced cytotoxicity in SH-SY5Y cells through preserving Akt/mTOR activity. *Drug Des. Dev. Ther.* **13**, 1659–1666. https://doi.org/10.2147/DDDT.S201122 (2019).
70. Sanchez-Alegria, K., Flores-Leon, M., Avila-Munoz, E., Rodriguez-Corona, N. & Arias, C. PI3K signaling in neurons: A central node for the control of multiple functions. *Int. J. Mol. Sci.* https://doi.org/10.3390/ijms19123725 (2018).
71. Shioda, N., Han, F. & Fukunaga, K. Role of Akt and ERK signaling in the neurogenesis following brain ischemia. *Int. Rev. Neurobiol.* **85**, 375–387. https://doi.org/10.1016/S0074-7742(09)85026-5 (2009).
72. Bruel-Jungerman, E. *et al.* Inhibition of PI3K-Akt signaling blocks exercise-mediated enhancement of adult neurogenesis and synaptic plasticity in the dentate gyrus. *PLoS One* **4**, e7901. https://doi.org/10.1371/journal.pone.0007901 (2009).
73. Sun, L., Cui, K., Xing, F. & Liu, X. Akt dependent adult hippocampal neurogenesis regulates the behavioral improvement of treadmill running to mice model of post-traumatic stress disorder. *Behav. Brain Res.* **379**, 112375. https://doi.org/10.1016/j.bbr.2019.112375 (2020).
74. Rozemuller, A. J., van Gool, W. A. & Eikelenboom, P. The neuroinflammatory response in plaques and amyloid angiopathy in Alzheimer's disease: Therapeutic implications. *Curr. Drug Targets CNS Neurol. Disord.* **4**, 223–233. https://doi.org/10.2174/1568007054038229 (2005).
75. Ransohoff, R. M. How neuroinflammation contributes to neurodegeneration. *Science* **353**, 777–783. https://doi.org/10.1126/science.aag2590 (2016).
76. Pike, C. J., Cummings, B. J. & Cotman, C. W. Early association of reactive astrocytes with senile plaques in Alzheimer's disease. *Exp. Neurol.* **132**, 172–179. https://doi.org/10.1016/0014-4886(95)90022-5 (1995).
77. Appel, J. R. *et al.* Increased microglial activity, impaired adult hippocampal neurogenesis, and depressive-like behavior in microglial VPS35-depleted mice. *J. Neurosci.* **38**, 5949–5968. https://doi.org/10.1523/JNEUROSCI.3621-17.2018 (2018).
78. Ekdahl, C. T., Claasen, J. H., Bonde, S., Kokaia, Z. & Lindvall, O. Inflammation is detrimental for neurogenesis in adult brain. *Proc. Natl. Acad. Sci. U. S. A.* **100**, 13632–13637. https://doi.org/10.1073/pnas.2234031100 (2003).
79. Zhang, J. *et al.* Priming of microglia with IFN-gamma impairs adult hippocampal neurogenesis and leads to depression-like behaviors and cognitive defects. *Glia* **68**, 2674–2692. https://doi.org/10.1002/glia.23878 (2020).
80. Monje, M. L., Toda, H. & Palmer, T. D. Inflammatory blockade restores adult hippocampal neurogenesis. *Science* **302**, 1760–1765. https://doi.org/10.1126/science.1088417 (2003).
81. Inestrosa, N. C. *et al.* Age progression of neuropathological markers in the brain of the chilean rodent *Octodon degus*, a natural model of Alzheimer's disease. *Brain Pathol.* **25**, 679–691. https://doi.org/10.1111/bpa.12226 (2015).
82. Ardiles, A. O. *et al.* Postsynaptic dysfunction is associated with spatial and object recognition memory loss in a natural model of Alzheimer's disease. *Proc. Natl. Acad. Sci. U. S. A.* **109**, 13835–13840. https://doi.org/10.1073/pnas.1201209109 (2012).
83. Cisternas, P. *et al.* New insights into the spontaneous human Alzheimer's disease-like model *Octodon degus*: Unraveling amyloid-beta peptide aggregation and age-related amyloid pathology. *J. Alzheimers Dis.* **66**, 1145–1163. https://doi.org/10.3233/JAD-180729 (2018).
84. Bilia, A. R. *et al.* Successful brain delivery of andrographolide loaded in human albumin nanoparticles to TgCRND8 mice, an Alzheimer's disease mouse model. *Front. Pharmacol.* **10**, 910. https://doi.org/10.3389/fphar.2019.00910 (2019).
85. Yang, R., Liu, S., Zhou, J., Bu, S. & Zhang, J. Andrographolide attenuates microglia-mediated Abeta neurotoxicity partially through inhibiting NF-kappaB and JNK MAPK signaling pathway. *Immunopharmacol. Immunotoxicol.* **39**, 276–284. https://doi.org/10.1080/08923973.2017.1344989 (2017).
86. Koo, J. W., Russo, S. J., Ferguson, D., Nestler, E. J. & Duman, R. S. Nuclear factor-kappaB is a critical mediator of stress-impaired neurogenesis and depressive behavior. *Proc. Natl. Acad. Sci. U. S. A.* **107**, 2669–2674. https://doi.org/10.1073/pnas.0910658107 (2010).
87. Beurel, E. Regulation by glycogen synthase kinase-3 of inflammation and T cells in CNS diseases. *Front. Mol. Neurosci.* **4**, 18. https://doi.org/10.3389/fnmol.2011.00018 (2011).
88. Deng, J. *et al.* beta-catenin interacts with and inhibits NF-kappa B in human colon and breast cancer. *Cancer Cell* **2**, 323–334. https://doi.org/10.1016/s1535-6108(02)00154-x (2002).
89. Ma, B. & Hottiger, M. O. Crosstalk between Wnt/beta-Catenin and NF-kappaB signaling pathway during inflammation. *Front. Immunol.* **7**, 378. https://doi.org/10.3389/fimmu.2016.00378 (2016).
90. Hollands, C. *et al.* Depletion of adult neurogenesis exacerbates cognitive deficits in Alzheimer's disease by compromising hippocampal inhibition. *Mol. Neurodegener.* **12**, 64. https://doi.org/10.1186/s13024-017-0207-7 (2017).
91. Richetin, K. *et al.* Genetic manipulation of adult-born hippocampal neurons rescues memory in a mouse model of Alzheimer's disease. *Brain* **138**, 440–455. https://doi.org/10.1093/brain/awu354 (2015).
92. Choi, S. H. *et al.* Combined adult neurogenesis and BDNF mimic exercise effects on cognition in an Alzheimer's mouse model. *Science* https://doi.org/10.1126/science.aan8821 (2018).
93. Varela-Nallar, L. *et al.* Chronic hypoxia induces the activation of the Wnt/beta-catenin signaling pathway and stimulates hippocampal neurogenesis in wild-type and APPswe-PS1DeltaE9 transgenic mice in vivo. *Front. Cell Neurosci.* **8**, 17. https://doi.org/10.3389/fncel.2014.00017 (2014).
94. Schindelin, J. *et al.* Fiji: An open-source platform for biological-image analysis. *Nat. Methods* **9**, 676–682. https://doi.org/10.1038/nmeth.2019 (2012).
95. Schafer, S. T. *et al.* The Wnt adaptor protein ATP6AP2 regulates multiple stages of adult hippocampal neurogenesis. *J. Neurosci.* **35**, 4983–4998. https://doi.org/10.1523/JNEUROSCI.4130-14.2015 (2015).
96. Arredondo, S. B. *et al.* Wnt5a promotes differentiation and development of adult-born neurons in the hippocampus by noncanonical Wnt signaling. *Stem Cells* **38**, 422–436. https://doi.org/10.1002/stem.3121 (2020).
97. Denninger, J. K., Smith, B. M. & Kirby, E. D. Novel object recognition and object location behavioral testing in mice on a budget. *J. Vis. Exp. JoVE* https://doi.org/10.3791/58593 (2018).
98. Jury, N. *et al.* Widespread loss of the silencing epigenetic mark H3K9me3 in astrocytes and neurons along with hippocampal-dependent cognitive impairment in C9orf72 BAC transgenic mice. *Clin. Epigenet.* **12**, 32. https://doi.org/10.1186/s13148-020-0816-9 (2020).

Acknowledgements

This work was supported by ANID/FONDECYT N°1190461 to LV-N, ANID/FONDECYT postdoctoral grant N°3200463 to AH-S.

Author contributions

S.B.A.: conception and design, collection and assembly of data, data analysis and interpretation and manuscript writing. D.R., A.H.-S., M.D.M.: Collection and assembly of data, data analysis and interpretation. N.C.I.: Conception and design, manuscript writing. L.V.-N.: Conception and design, data analysis and interpretation, manuscript writing. All authors approved the final version as submitted.

Competing interests
The authors declare no competing interests.

Additional information
Supplementary Information The online version contains supplementary material available at https://doi.org/10.1038/s41598-021-01977-x.

Correspondence and requests for materials should be addressed to N.C.I. or L.V.-N.

Reprints and permissions information is available at www.nature.com/reprints.

Publisher's note Springer Nature remains neutral with regard to jurisdictional claims in published maps and institutional affiliations.